Generalized acoustic energy density

Buye Xu,[a)] Scott D. Sommerfeldt, and Timothy W. Leishman
Department of Physics and Astronomy, Brigham Young University, Provo, Utah 84602

(Received 15 September 2010; revised 8 July 2011; accepted 21 July 2011)

The properties of acoustic kinetic energy density and total energy density of sound fields in lightly damped enclosures have been explored thoroughly in the literature. Their increased spatial uniformity makes them more favorable measurement quantities for various applications than acoustic potential energy density (or squared pressure), which is most often used. In this paper, a generalized acoustic energy density (GED), will be introduced. It is defined by introducing weighting factors into the formulation of total acoustic energy density. With an additional degree of freedom, the GED can conform to the traditional acoustic energy density quantities, or it can be optimized for different applications. The properties of the GED will be explored in this paper for individual room modes, a diffuse sound field, and a sound field below the Schroeder frequency.
 [DOI: 10.1121/1.3624482]

PACS number(s): 43.55.Br, 43.20.Ye, 43.55.Cs, 43.50.Ki [SFW] Pages: 1370–1380

I. INTRODUCTION

Since the pioneering work by Sabine,[1] measurements based on acoustic pressure, squared pressure, or acoustic potential energy density have become a primary focus for room acoustics. In the early 1930s, Wolff experimentally studied the kinetic energy density as well as total energy density in a room with the use of pressure gradient microphones.[2,3] His results indicated a better spatial uniformity of both the kinetic energy density and total energy density over the potential energy density.

In 1974, the preliminary experimental study by Sepmeyer *et al*.[4] showed that for a pure-tone diffuse sound field, the potential energy density has a relative spatial variance of 1, which is consistent with the theoretical results by Waterhouse[5] and Lyon.[6] In addition, they also found that the variance of potential energy density is approximately twice that of the total energy density. In the same year, Cook *et al.* showed that the spatial variance of total energy density is smaller than that of the squared pressure for standing waves.[7]

Following Waterhouse's free-wave concept,[8,9] Jacobsen studied the statistics of acoustic energy density quantities from a stochastic point of view.[10] Moryl *et al*.[11,12] experimentally investigated the relative spatial standard deviation of acoustic energy densities in a pure tone reverberant field with a four-microphone probe. Their results are in fair agreement with Jacobsen's prediction.

Jacobsen, together with Molares, revised his 1979 results[10] by applying the weak Anderson localization arguments,[13] and they were able to extend the free-wave model to low frequencies.[14,15] The new formulas for sound power radiation variance and ensemble variance of pure-tone excitations are very similar to those derived from the modal model,[6,16,17] but with a simpler derivation. The same authors then investigated the statistical properties of kinetic energy density and total acoustic energy density in the low frequency range.[18]

[a)]Author to whom correspondence should be addressed. Electronic mail: buye.xu@gmail.com

The pressure microphone gradient technique for measuring acoustic energy quantities has been studied and improved over time.[3,4,11,19–22] Recently, a novel particle velocity measurement device, Microflown, has been made available to acousticians,[23,24] expanding the methods available to measure acoustic energy density quantities. More and more attention is consequently being devoted to their study and use.

By recognizing the increased uniformity of the total energy density field, Parkins *et al*. implemented active noise control (ANC) by minimizing the total energy density in enclosures. Significant attenuation was achieved at low frequencies.[25,26] In 2007, Nutter *et al*. investigated acoustic energy density quantities for several key applications in reverberation chambers and explored the benefits introduced by the uniformity of both kinetic energy density and total acoustic energy density.[27]

Most studies of kinetic energy density and total energy density have focused on their improved uniformity in reverberant sound fields. A new energy density quantity, the generalized acoustic energy density (GED), will be introduced in this paper and shown to be more uniform than all other commonly used acoustic energy density quantities. Yet it requires no more effort to obtain than kinetic energy and total energy density.

The paper will be organized as follows. The GED and some of its general properties will be introduced in Sec. II. In Sec. III its behavior will be explored for room modes. Its properties in a diffuse field will be investigated in Sec. IV with a focus on single-tone excitation and certain characteristics of narrow-band excitation. In Sec. V its spatial variance will be studied for frequencies below the Schroeder frequency of a room. Computer simulation results will be presented in Sec. VI to validate some of the GED properties introduced in the paper. In Sec. VII three applications of the GED will be studied experimentally and numerically.

II. GENERALIZED ENERGY DENSITY

The total acoustic energy density is defined as the acoustic energy per unit volume at a point in a sound field. The

 0001-4966/2011/130(3)/1370/11/$30.00

time-averaged total acoustic energy density can be expressed in the frequency domain as

$$E_T = E_P + E_K = \frac{1}{2}\frac{pp^*}{\rho_0 c^2} + \frac{1}{2}\rho_0 \mathbf{u}\cdot\mathbf{u}^*, \tag{1}$$

where p and $\mathbf{u}$ represent the complex acoustic pressure and particle velocity, respectively, in the frequency domain, ρ_0 is the ambient fluid density, and c is the speed of sound. On the right-hand side of this expression, the first term represents the time-averaged potential energy density (E_P) and the second term represents the time-averaged kinetic energy density (E_K). The time-averaged kinetic energy density can be written as the sum of three orthogonal components as

$$E_K = E_{Kx} + E_{Ky} + E_{Kz} = \frac{1}{2}\rho_0 u_x u_x^* + \frac{1}{2}\rho_0 u_y u_y^* + \frac{1}{2}\rho_0 u_z u_z^*. \tag{2}$$

The GED is defined as follows:

$$E_{G(\alpha)} = \alpha E_P + (1-\alpha)E_K, \tag{3}$$

where α is an arbitrary real number. The GED is simply the sum of E_P and E_K with weighting factors that add to 1. One can cause the GED to represent the traditional energy density quantities by appropriately varying α. In other words, $E_P = E_{G(1)}$, $E_K = E_{G(0)}$, and $E_T = 2E_{G(1/2)}$. Although, in theory, α could be any real number, the range $0 \le \alpha \le 1$ will be the focus of this work, because it contains all values of α that make GED favorable for the applications studied herein. However, most theoretical derivations presented in this paper are general enough that the results can be implemented directly for the entire domain of real numbers.

The spatial mean of GED for a sound field can be calculated as

$$\mu_G = E[E_G] = E[\alpha E_P + (1-\alpha)E_K] = \alpha\mu_P + (1-\alpha)\mu_K, \tag{4}$$

where $E[\cdots]$ represents the expectation operator and μ_G, μ_P, and μ_K represent the spatial mean value of E_G, E_P, and E_K, respectively. Given that $\mu_P = \mu_K$ for most enclosed sound fields,[10] one can conclude from Eq. (4) that μ_G does not vary due to α, and $\mu_G = \mu_P = \mu_K$.

The relative spatial variance of GED can similarly be calculated as

$$\begin{aligned}\epsilon_G^2 &= \frac{\sigma^2[E_G]}{E^2[E_G]} = \frac{E[E_G^2] - E^2[E_G]}{E^2[E_G]} \\ &= \frac{\alpha^2 E[E_P^2] + 2\alpha(1-\alpha)E[E_P E_K] + (1-\alpha)^2 E[E_K^2] - \mu_G^2}{\mu_G^2} \\ &= \frac{\alpha^2(E[E_P^2]-\mu_P^2)}{\mu_P^2} + \frac{(1-\alpha)^2(E[E_K^2]-\mu_K^2)}{\mu_K^2} \\ &\quad + \frac{2\alpha(1-\alpha)(E[E_P E_K]-\mu_P\mu_K)}{\mu_P\mu_K} \\ &= \alpha^2\epsilon_P^2 + (1-\alpha)^2\epsilon_K^2 + 2\alpha(1-\alpha)\epsilon_{PK}^2, \end{aligned} \tag{5a}$$

$$= \alpha^2(\epsilon_P^2 + \epsilon_K^2 - 2\epsilon_{PK}^2) + 2\alpha(\epsilon_{PK}^2 - \epsilon_K^2) + \epsilon_K^2, \tag{5b}$$

where $\sigma^2[\cdots]$ represents the spatial variance; ϵ_G^2, ϵ_P^2, and ϵ_K^2 represent the relative spatial variances of E_G, E_P, and E_K respectively; and ϵ_{PK}^2 represents the relative spatial co-variance of E_P and E_K. In the derivation of the equations above, the relations of $\mu_G = \alpha\mu_P + (1-\alpha)\mu_K$ and $\mu_G = \mu_P = \mu_K$ are utilized. One can show by substituting appropriate values for α that Eq. (5a) can revert to ϵ_P ($\alpha = 1$) and ϵ_K ($\alpha = 0$). Equation (5b) shows that the relative variance of GED is a quadratic function of α. In addition, recognizing that $\epsilon_P^2 + \epsilon_K^2 > 2\epsilon_{PK}^2$, one can conclude that ϵ_G^2 has a global minimum,

$$\min\{\epsilon_G^2\} = \frac{\epsilon_P^2\epsilon_K^2 - \epsilon_{PK}^4}{(\epsilon_P^2 + \epsilon_K^2 - 2\epsilon_{PK}^2)}, \tag{6}$$

when

$$\alpha = \frac{(\epsilon_K^2 - \epsilon_{PK}^2)}{(\epsilon_P^2 + \epsilon_K^2 - 2\epsilon_{PK}^2)}. \tag{7}$$

As explained in the following discussion, the kinetic energy density and total energy density may not be the most spatially uniform quantities.

III. MODAL ANALYSIS

Below the Schroeder frequency, distinct room modes often dominate an enclosed sound field. Consider a hard-walled rectangular room with dimensions $L_x \times L_y \times L_z$, with a single mode dominating the response at a resonance frequency. Ignoring any constants, E_P and E_K can be expressed approximately as[28]

$$E_P = \cos^2(k_x x)\cos^2(k_y y)\cos^2(k_z z), \tag{8a}$$

$$\begin{aligned}E_K &= \frac{k_x^2\sin^2(k_x x)\cos^2(k_y y)\cos^2(k_z z)}{k^2} \\ &\quad + \frac{k_y^2\cos^2(k_x x)\sin^2(k_y y)\cos^2(k_z z)}{k^2} \\ &\quad + \frac{k_z^2\cos^2(k_x x)\cos^2(k_y y)\sin^2(k_z z)}{k^2},\end{aligned} \tag{8b}$$

where k_x, k_y, and k_z are eigenvalues and $k^2 = k_x^2 + k_y^2 + k_z^2$.

For an axial mode, where two of the three eigenvalues vanish (assumed here in the y and z directions),

$$E_G = \alpha\cos^2(kx) + (1-\alpha)\sin^2(kx), \quad \epsilon_G^2 = 2\alpha^2 - 2\alpha + \frac{1}{2}. \tag{9}$$

With no surprise, the relative variance reaches its minimum value of zero when $\alpha = 1/2$, which corresponds to the total acoustic energy density being uniform for an axial mode.

For a tangential mode (only 1 eigenvalue equals zero), the expression for the relative variance is not as simple as that for an axial mode. It depends on both α and the ratio

TABLE I. Relative variance of single modes.

Mode	μ	ϵ_P^2	ϵ_G^2
Axial	1/2	1/2	$\frac{(2\alpha-1)^2}{2}$
Tangential	1/4	5/4	$\frac{5-6\gamma^2+5\gamma^4-4(3-2\gamma^2+3\gamma^4)\alpha+4(3+2\gamma^2+3\gamma^4)\alpha^2}{4(1+\gamma^2)^2}$
Oblique	1/8	19/8	$\frac{19-10\gamma_{xy}^2(1+\gamma_{yz}^2)+\gamma_{xy}^4(19-10\gamma_{yz}^2+19\gamma_{yz}^4)}{8\left(1+\gamma_{xy}^2+\gamma_{xy}^2r_2^2\right)^2} - \frac{[3-2\gamma_{xy}^2(1+\gamma_{yz}^2)+\gamma_{xy}^4(3-2\gamma_{yz}^2+3\gamma_{yz}^4)]\alpha}{2\left(1+\gamma_{xy}^2+\gamma_{xy}^2r_2^2\right)^2} + \frac{[3+2\gamma_{xy}^2(1+\gamma_{yz}^2)+\gamma_{xy}^4(3+2\gamma_{yz}^2+3\gamma_{yz}^4)]\alpha^2}{2\left(1+\gamma_{xy}^2+\gamma_{xy}^2r_2^2\right)^2}$

$\gamma = k_y/k_x$ (assuming $k_z = 0$), as shown in Table I. Some examples of the spatial variance for different γ values are shown in Fig. 1(a). By assuming $k_x \le k_y$, it is not difficult to prove that ϵ_G^2 increases with γ for all α values less than 1, and as γ tends to infinity, ϵ_G^2 converges to

$$\epsilon_G^2\big|_{\gamma\to\infty} = \frac{5}{4} - 3\alpha + 3\alpha^2. \tag{10}$$

The optimized value of α, which minimizes the relative variance, ranges between 1/4, when $\gamma = 1$, and 1/2, when $\gamma \to \infty$. With the optimal α value, the relative variance can become a tenth that of E_P and half that of E_T.

For an oblique mode, the relative variance again depends on α as well as all the eigenvalues. With ratios $\gamma_{xy} = k_y/k_x$ and $\gamma_{yz} = k_z/k_y$, one can derive the expression for ϵ_G^2 shown in Table I. When γ_{xy} approaches infinity while γ_{yz} remains finite, the behavior of ϵ_G^2 is very similar to that of the tangential modes. As a limiting case, when $\gamma_{xy} \to \infty$ and $\gamma_{yz} = 1$, ϵ_G^2 converges to

$$\epsilon_G^2\big|_{\gamma_{xy}\to\infty,\gamma_{yz}=1} = \frac{7}{8} - \frac{3\alpha}{2} + 3\alpha^2, \tag{11}$$

which, similar to the tangential mode with $\gamma = 1$, reaches the minimum when $\alpha = 1/4$. As the value γ_{yz} approaches infinity, ϵ_G^2 converges to

$$\epsilon_G^2\big|_{\gamma_{yz}\to\infty} = \frac{19}{8} - \frac{9\alpha}{2} + \frac{9\alpha^2}{2}, \tag{12}$$

regardless of the value of γ_{xy} [see Fig. 1(b)]. The optimal α value varies from 1/10 to 1/2 depending on the values of γ_{xy} and γ_{yz}. However, as can be observed from Fig. 1(c), if $\gamma_{yz} < 2$ the optimal α value is generally in the range of 0.1 to 0.35. With the optimal α value, the relative variance can become a factor of 6.8 smaller than that of E_P and half that of E_T. It is interesting to note that for all possible values of γ, γ_{xy}, and γ_{yz}, E_P has the highest relative variance, which is a constant for each type of mode.

IV. GED IN DIFFUSE FIELDS

The free-wave model[5] has been successfully used to study the statistical properties of diffuse sound fields. It assumes that

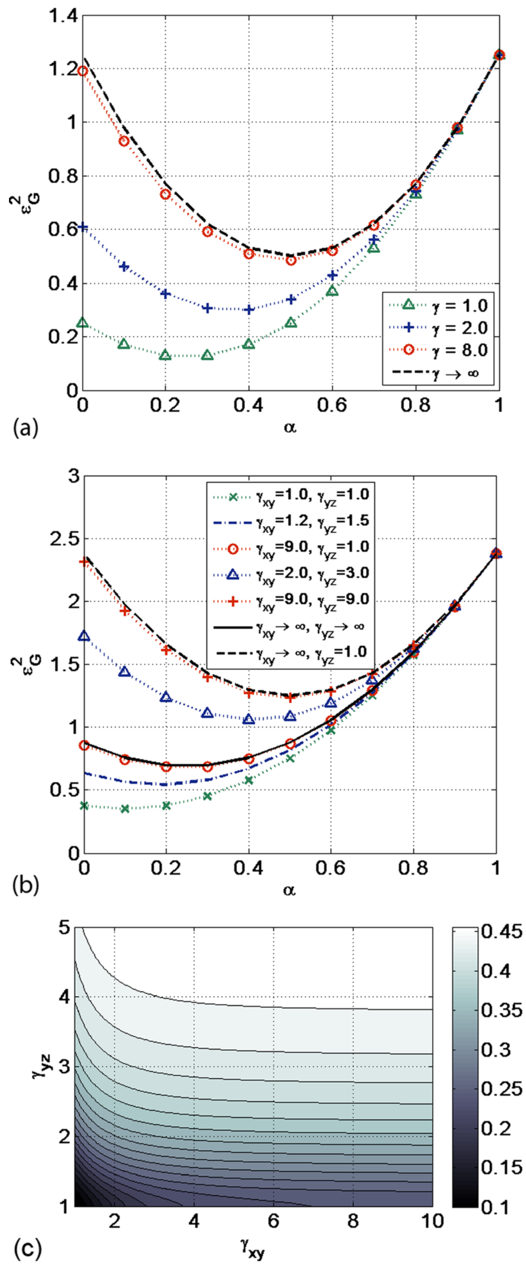

FIG. 1. (Color online) Relative spatial variance of GED for (a) a tangential mode and (b) an oblique mode. The contour plot (c) shows the optimal values of α that minimize ϵ_G^2 for the oblique modes.

the sound field at any arbitrary point is composed of a large number of plane waves with random phases and directions. For a single-tone field, the complex acoustic pressure amplitude for a given frequency can thus be written as

$$p = \sum_m A_m e^{i(k\mathbf{n}_m\cdot\mathbf{r}+\phi_m)}, \quad (13)$$

where A_m is a random real number representing the peak amplitude of the mth wave, and the unit vector $\mathbf{n}_m$ and phase ϕ_m are uniformly distributed in their spans.

It can be shown, based on the central limit theorem, that the rms value of squared pressure has an exponential distribution,[5,10] and the probability density function (PDF) of E_p is

$$f_{E_P}(x) = \frac{1}{\mu_G} e^{-x/\mu_G}; \quad x \geq 0. \quad (14)$$

The mean and variance are μ_G and μ_G^2, respectively, for the exponentially distributed E_P, so the relative variance is 1.

Using a similar argument, Jacobsen was able to show that the three components of kinetic energy density (E_{Kx}, E_{Ky}, and E_{Kz}) are independent and follow an exponential distribution. Therefore, the kinetic energy density is distributed as $\Gamma(3, \mu_G/3)$,[10] and the PDF is

$$f_{E_K}(x) = \frac{27x^2 e^{-3x/\mu_G}}{2\mu_G^3}; \quad x > 0. \quad (15)$$

The mean and variance for this distribution are μ_G and $\mu_G^2/3$, respectively, and the relative variance is $1/3$, which is significantly less than that of the potential energy density.

Because E_P and E_K are independent,[10] one can compute the cumulative distribution function (CDF) and PDF for the GED with the following equations:

$$F_{E_G}(x) = \int_0^{x/\alpha} f_{E_P}(y) \int_0^{(x-\alpha y)/(1-\alpha)} f_{E_K}(z)dzdy, \quad (16)$$

$$f_{E_G}(x) = \frac{dF_{E_G}(x)}{dx}. \quad (17)$$

The calculation is rather involved, so only the final result for the PDF will be shown here:

$$f_{E_G}(x) = \frac{27\alpha^2\left(e^{-3x/\mu_G(1-\alpha)} - e^{-x/(\mu_G\alpha)}\right)}{\mu_G(1-4\alpha)^3} + \frac{27x[x(1-4\alpha) - 2\mu_G\alpha(1-\alpha)]e^{-3x/\mu_G(1-\alpha)}}{2\mu_G^3(1-\alpha)^2(1-4\alpha)^2}. \quad (18)$$

It is not hard to show that Eq. (18) converges to Eq. (14) and Eq. (15) for the limiting cases wherein $\alpha \to 1$ and $\alpha \to 0$, respectively.

With the use of Eq. (18) [or Eq. (5a)], one can obtain the relative spatial variance

$$\epsilon_G^2 = \frac{1}{3}(4\alpha^2 - 2\alpha + 1), \quad (19)$$

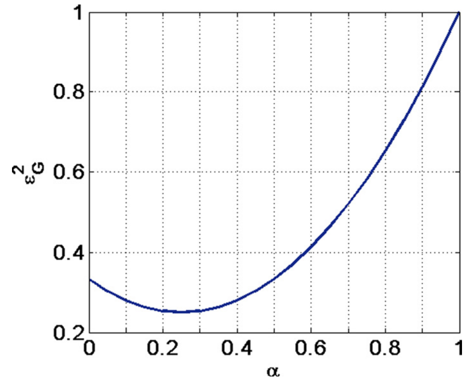

FIG. 2. (Color online) Relative spatial variance of GED in a diffuse field. The minimum variance is reached at $\alpha = 1/4$.

as plotted in Fig. 2. The minimum relative variance is $1/4$ when $\alpha = 1/4$. At this optimal α value, the distribution of the GED turns out to be simply $\Gamma(4, \mu_G/4)$, which should not be surprising if it is rewritten as

$$\begin{aligned} E_{G(1/4)} &= \frac{1}{4}E_P + \frac{3}{4}E_K \\ &= \frac{1}{4}E_P + \frac{3}{4}(E_{Kx} + E_{Ky} + E_{Kz}) \\ &= \frac{3}{4}(E_P/3 + E_{Kx} + E_{Ky} + E_{Kz}), \end{aligned} \quad (20)$$

which is essentially the sum of four independent $\Gamma(1, \mu_G/3)$ random variables multiplied by a shape factor of $3/4$.

For narrow-band excitation, the relative spatial variance of the GED is approximately equal to the relative spatial variance for the single-tone excitation multiplied by $(1 + BT_{60}/6.9)^{-1}$, where B is the bandwidth and T_{60} represents the reverberation time.[29]

The spatial correlation between pressures at two separated field points in a single-tone diffuse field was first studied by Cook and Waterhouse.[30] At any arbitrary time t, the spatial correlation coefficient between $p_1 = p(\mathbf{r}_1, t)$ and $p_2 = p(\mathbf{r}_2, t)$ can be calculated as

$$\begin{aligned} \rho_p(r) &= \frac{\mathrm{Cov}[p_1, p_2]}{\sigma[p_1]\sigma[p_2]} \\ &= \frac{\sin(kr)}{kr}, \end{aligned} \quad (21)$$

where $\sigma[\cdots]$ represents standard deviation, k is the wave number, and $r = |\mathbf{r}_2 - \mathbf{r}_1|$. Lubman[31] obtained a formula for the spatial correlation coefficients for the squared pressures and E_P:

$$\rho_{E_P} = \rho_{p^2} = \left[\frac{\sin(kr)}{kr}\right]^2. \quad (22)$$

Jacobsen[10] later derived the formulas for squared particle velocity components, as well as squared velocity and squared pressure. These formulas can be applied to E_K and E_P directly to obtain the spatial autocorrelation and cross correlation coefficients:

$$\rho_{E_K} = \rho_{u^2} = \frac{3(6+2k^2r^2+k^4r^4)}{2k^6r^6} + \frac{3[4kr(-3+k^2r^2)\sin(2kr) - (6-10k^2r^2+k^4r^4)\cos(2kr)]}{2k^6r^6}, \tag{23}$$

$$\rho_{E_P,E_K} = \rho_{p^2,u^2} = \sqrt{3}\left[\frac{\sin(kr) - kr\cos(kr)}{(kr)^2}\right]^2. \tag{24}$$

The spatial correlation coefficient for the GED at two field points can then be calculated as

$$\rho_{E_G} = \frac{1}{\epsilon_G^2}\left[\alpha^2\epsilon_P^2\rho_{E_P} + \alpha(1-\alpha)\epsilon_P\epsilon_K\rho_{E_P,E_K} + (1-\alpha)^2\epsilon_K^2\rho_{E_K}\right], \tag{25}$$

where $\epsilon_P^2 = 1$ and $\epsilon_K^2 = 1/3$, as indicated earlier. Note that ρ_{E_G}, as ρ_{E_P} and ρ_{E_K}, is also a function of r, although it is not shown explicitly in Eq. (25). There is not a concise expression for ρ_{E_G}, but some examples for different values of α are plotted in Fig. 3. It is well accepted that the spatial correlation can be neglected for the potential energy density if the distance between two field points is greater than half a wavelength (0.5λ).[10] In order to achieve a similarly low level of correlation (roughly $\rho \leq 0.05$), the separation distance needs to be greater than approximately 0.8λ for E_K, E_T, and $E_{G(1/4)}$. This may not be favorable for some applications, such as sound power measurements in a reverberant room, because statistically independent sampling is required. It is, in some sense, a trade off for achieving better uniformity. However, for other applications, i.e., active noise control in diffuse fields,[32] a slowly decaying spatial correlation function may be beneficial.

As one approaches the regions close to boundaries, it is hard to claim a truly diffuse field even if the frequency is well above the Schroeder frequency in a reverberation chamber. Because of the strong reflections, one would expect some kind of interference effects. Waterhouse obtained expressions for the mean-squared pressure, mean-squared velocity and mean total energy density as functions of the distance from the boundaries.[33] His results can be directly applied to E_P and E_K. For a sound field close to a flat rigid boundary, one has

$$\langle E_P\rangle/\mu_G = 1 + \frac{\sin(2kx)}{2kx}, \tag{26}$$

$$\langle E_K\rangle/\mu_G = 1 - \frac{\sin(2kx)}{2kx} + \frac{\sin(2kx) - 2kx\cos(2kx)}{2(kx)^3}, \tag{27}$$

and, thus,

$$\begin{aligned}\langle E_G\rangle/\mu_G &= (\alpha E_P + (1-\alpha)E_K)/\mu_G \\ &= \alpha\left[1 + \frac{\sin(2kx)}{2kx}\right] + (1-\alpha)\left[1 - \frac{\sin(2kx)}{2kx} + \frac{\sin(2kx) - 2kx\cos(2kx)}{2(kx)^3}\right] \\ &= 1 + \frac{2kx(-1+\alpha)\cos(2kx) + [1-\alpha-k^2x^2(1-2\alpha)]\sin(2kx)}{2k^3x^3},\end{aligned} \tag{28}$$

where x represents the distance from the boundary, $\langle\cdots\rangle$ represents a spatial average on the surface that is the distance x away from the boundary, and μ_G refers to the mean of GED in the region that is far away from all boundaries. As shown in Fig. 4, all the GED quantities have higher mean values at the boundary, and as the distance increases, the mean values converge to μ_G fairly quickly after half a wave length.

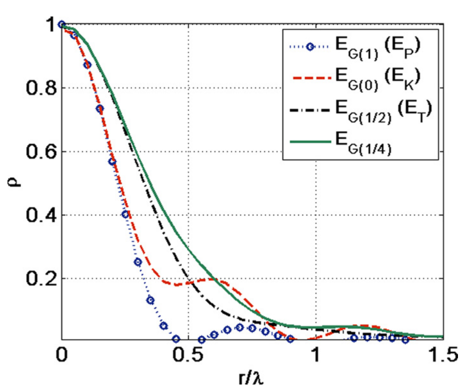

FIG. 3. (Color online) Spatial correlation coefficient ρ of different GED quantities in a diffuse field.

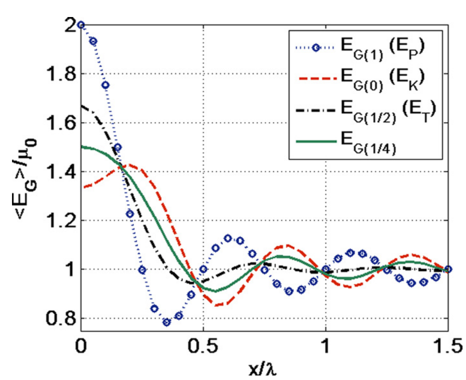

FIG. 4. (Color online) Mean values of different GED quantities as a function of the distance x from a flat rigid boundary in a diffuse field.

Jacobsen rederived similar results from the stochastic perspective, and found that both the potential energy density and all components of kinetic energy density near a boundary (either perpendicular or parallel to the boundary) are independently distributed with the exponential distribution.[10] Therefore, the relative variance of GED near a boundary can be shown to be

$$\epsilon_{E_G}^2(x) = \frac{\alpha^2\sigma_{E_P}^2(x) + (1-\alpha)^2\sigma_{E_K}^2(x)}{(E_G)^2}, \tag{29}$$

where

$$\sigma_{E_P}^2(x)=(E_P)^2,$$
$$\sigma_{E_K}^2(x)=(E_{K_\perp})^2+2\left(E_{K_\parallel}\right)^2 \tag{30}$$
$$=\left[\frac{1}{3}+\frac{-2kx\cos(2kx)+\sin(2kx)}{8k^3x^3}\right]^2 + \left[\frac{1}{3}-\frac{4kx\cos(2kx)-2\sin(2kx)+4k^2x^2\sin(2kx)}{8k^3x^3}\right]^2, \tag{31}$$

where $E_{K_\perp}$ represents the component of E_K perpendicular to the boundary, and $E_{K_\parallel}$ represents the component parallel to the boundary.[10] Immediately adjacent to the boundary ($x \to 0$), Eq. (29) can be simplified to the form

$$\epsilon_{E_G}^2(0) = \frac{2-4\alpha+11\alpha^2}{(2+\alpha)^2}, \tag{32}$$

which has a minimum value of $1/3$ at $\alpha = 1/4$. Figure 5 plots Eqs. (29) and (32). It is apparent that $E_{G(1/4)}$ is more uniform than E_P, E_K, and E_T everywhere, both near the boundary and in the region away from the boundary where a diffuse sound field can be claimed.

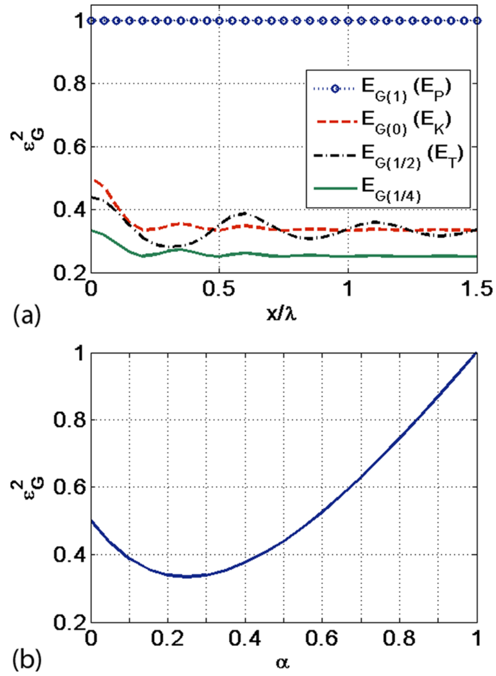

FIG. 5. (Color online) Relative spatial variance of GED close to a flat rigid boundary bounding a diffuse field. Plot (a) compares the relative variance for different GED quantities as a function of the distance x from the boundary. Plot (b) shows the relative variance of GED as a function of α at the boundary ($x \to 0$).

V. ENSEMBLE VARIANCE

In a recent publication, Jacobsen obtained the ensemble variance for the potential, kinetic, and total energy densities by introducing an independent normally distributed random variable W to the diffuse field models discussed previously.[15] The variable W has zero mean and a variance of $2/M_s$, and is meant to represent the relative variance of the point source sound power emission associated with the statistical modal overlap M_s.[15] Following his approach, the relative ensemble variance of GED can be expressed as

$$\begin{aligned}\epsilon_{E_G}^2 &= \frac{E\left([\alpha E_P + (1-\alpha)(E_{Kx}+E_{Ky}+E_{Kz})]^2(1+W)^2\right)}{E^2\left[[\alpha E_P + (1-\alpha)(E_{Kx}+E_{Ky}+E_{Kz})](1+W)\right]} - 1 \\ &= \frac{3(1-\alpha)^2\left(E\left[E_{Kx}^2\right]+2E^2[E_{Kx}]\right)+\alpha^2E\left[E_P^2\right]+6\alpha(1-\alpha)E[E_P]E[E_{Kx}]}{\mu_G^2}\left(1+E\left[W^2\right]\right)-1 \\ &= \left[\frac{4}{3}(1-\alpha)^2+2\alpha^2+2\alpha(1-\alpha)\right]\left(1+\frac{2}{M_s}\right)-1 \\ &= \frac{8+M_s-2(2+M_s)\alpha+4(2+M_s)\alpha^2}{3M_s}.\end{aligned} \tag{33}$$

It is interesting to note that the optimal α value is again $1/4$, and the minimum variance is $1/4 + 5/2M_s$, compared to $1 + 4/M_s$ for E_P and $1/3 + 8/3M_s$ for both E_K and E_T.

The modal overlap can be calculated according to

$$M_s = \frac{12\pi\ln(10)Vf^2}{T_{60}c^3}, \tag{34}$$

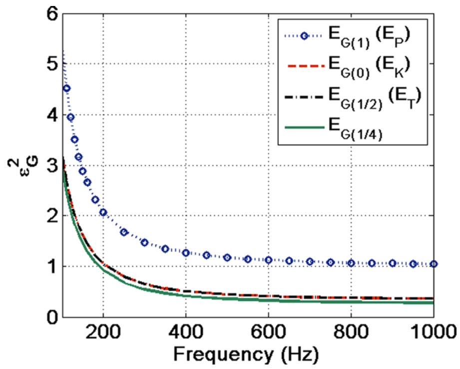

FIG. 6. (Color online) Ensemble variance of different GED quantities for a reverberation chamber with $V = 136.6$ m^2 and uniform $T_{60} = 6.2$ s.

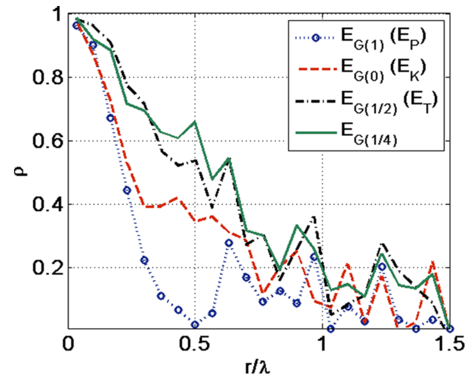

FIG. 8. (Color online) Numerical simulation results for the spatial correlation coefficient of GED in a diffuse field.

where V is the volume of the room and T_{60} is the reverberation time.[14] Figure 6 plots Eq. (33) for a room with volume 136.6 m^3 and a T_{60} of 6.2 s that is constant over frequency.

VI. NUMERICAL VERIFICATION

A hybrid modal expansion model[34] was applied to compute the internal sound field (both complex pressure and complex particle velocity) of a rectangular room with dimensions 5.4 m × 6.3 m × 4.0 m. The room is very lightly damped with a uniform wall impedance $z = (50 + 100i)\rho_0 c$ and a Schroeder frequency of 347.6 Hz. Both the complex pressure and complex particle velocity fields are computed over the bandwidth of 50–1000 Hz with 1 Hz increment. Because of the fast convergence rate of the hybrid model, only about 3×10^4 modes were required for even the highest frequency. The source location was randomly selected for each frequency.

The relative variance of E_G with different α values is estimated by calculating the relative variance for E_G at 100 randomly selected receiver locations inside the room. The receiver locations are chosen to be at least a half wavelength away from the source as well as the boundary. The relative variance for 100 samples is then averaged over ten frequency bins to simulate the ensemble variance.[15,18] As shown in Fig. 7, the simulation results match the theoretical predictions reasonably well (compare Fig. 6). The variation of the curves in Fig. 7 is due to the modal effects. Strictly speaking, in order to simulate the ensemble variance, a large (ideally infinite) number of rooms that vary in dimensions need to be considered. Averaging over a frequency band can only compensate for the lack of room variation to some degree.

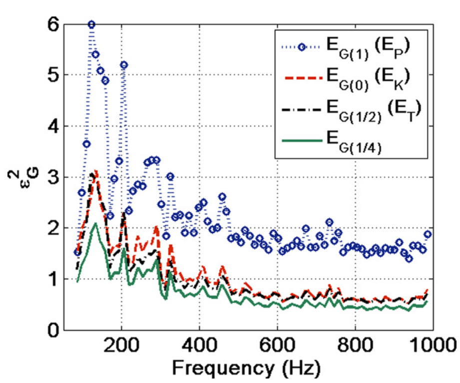

FIG. 7. (Color online) Numerical simulation results for the ensemble variance of different GED quantites for a lightly damped room.

The spatial correlation coefficient was estimated at 800 Hz using 11 000 pairs of field points randomly sampled with the constraint that the separation distance between any two points of a pair is less than one and a half wavelengths. In addition, the sampling process was carefully designed so there were about 500 pairs falling into each of 22 intervals that equally divided one and a half wavelengths. The spatial correlation coefficient was calculated for each interval based on the samples. The results are shown in Fig. 8. Although the frequency (800 Hz) is above the Schroeder frequency (347.6 Hz), the sound field still does not correspond to an ideal diffuse field; therefore some variations are apparent in the numerical results. Nonetheless, in general, the simulation results are in fairly good agreement with the theoretical predictions shown in Fig. 3.

VII. APPLICATIONS

One of the key elements of many applications in a reverberation chamber is the estimation of the statistical mean of the sound field based on a finite number of sampling locations. Two somewhat contradictory requirements, however, have to be met in order to achieve a good estimation: (1) the sound field being sampled at a sufficient number of locations to achieve the desired level of uncertainty and (2) the choice of the locations being random, independent, and limited to the diffuse field region to eliminate bias. Historically, squared pressure has been the predominant measurement focus in reverberation chambers, because it is relatively easy to measure. However, because of its larger spatial variance, its use does not help resolve the conflict stated above and may end up either requiring more effort to select measurement locations or a sacrifice in accuracy. Based on the capability of GED to achieve smaller spatial variance, the following preliminary studies have demonstrated its utility in acoustical measurements and active noise control.

A. Reverberation time estimation

In the paper by Nutter *et al.*,[27] the procedure of the reverberation time (T_{60}) estimation based on the total acoustic energy density is investigated in detail. It was shown for varying numbers of sensor locations that a small number of energy density measurements can achieve the same accuracy as larger numbers of pressure measurements. The impulse responses of multiple source-receiver locations were obtained for both acoustic pressure and particle velocity, from which an impulse response associated with the total energy density, h_{E_T}, was computed as

$$h_{E_T}(t) = \frac{1}{2\rho_0 c^2} h_p^2(t) + \frac{\rho_0}{2} h_u^2(t), \tag{35}$$

where h_p and h_u represent the impulse responses of acoustic pressure and particle velocity, respectively. The filtered impulse for each frequency band of interest was then backward integrated to reduce the estimation variance.[35] After averaging the backward integrated curves for the source-receiver combinations, T_{60} values could be estimated from the slopes of the averaged curves. To utilize GED, the procedure is very much the same, except that the impulse response associated with GED is calculated by changing the coefficients in Eq. (35) from $1/2$ to α and $1-\alpha$ for the first and second terms, respectively.

Reverberation times were thus obtained for a reverberation chamber based on GED with different values of α. The reverberation chamber dimensions were 4.96 m $\times$ 5.89 m $\times$ 6.98 m. Its volume was 204 m^3 and it incorporated stationary diffusers. The Schroeder frequency for the chamber was 410 Hz without the presence of low-frequency absorbers. A dodecahedron loudspeaker was placed sequentially at two locations within the chamber and driven by white noise. The acoustic pressure and particle velocity fields were sampled with a GRAS six-microphone probe at six chamber locations for each source location. The probe consisted of three pairs of phase-matched 1/2-inch microphones mounted perpendicular to each other with spacers, so three orthogonal particle velocity components could be estimated based on the pressure differences. The spacing between microphones in each pair was 5 cm, which is optimal for the frequencies below 1000 Hz. The acoustic pressure was estimated by averaging the pressure signals from all six microphones in the probe.

The impulse responses were computed by taking the inverse Fourier transform of the frequency responses between the acoustic pressure or particle velocity signals and the white noise signal input to the source. Technically, these impulse responses represent responses of both the chamber and the dodecahedron loudspeaker. However, the impulse response of the loudspeaker was too short to appreciably influence the T_{60} estimations. The impulse responses were filtered with one-third-octave band filters and backward integrated to estimate the T_{60} values within the bands. Figure 9(a) compares the averaged T_{60} estimation based on GED with different α values. The various GED quantities result in almost identical reverberation times in most one-third-octave bands. However, the variance due to source-receiver locations differs, especially in the low frequency range. As shown in Fig. 9(b), the estimations based on E_K, E_T, and $E_{G(1/4)}$ have notably less variance than E_P. Less variance implies a smaller number of measurements or better accuracy. Although the improvement

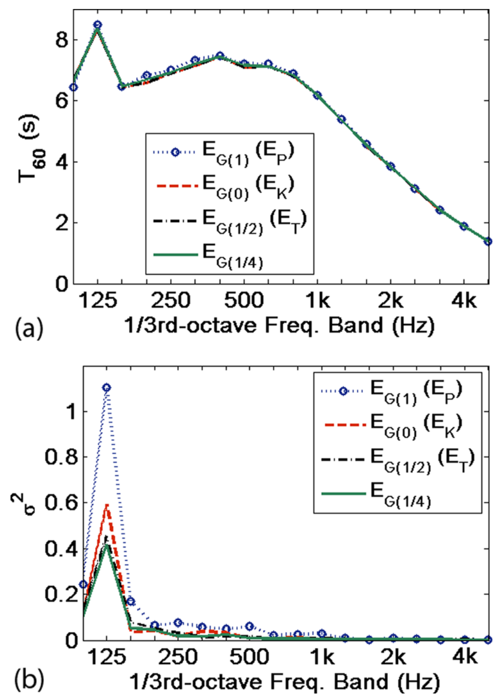

FIG. 9. (Color online) Reverberation time measurements using GED. (a) Averaged T_{60} estimation based on different GED quantities for a reverberation chamber. (b) Variance of the T_{60} estimations due to the different source-receiver locations.

over E_K and E_T is not large, the variance is the smallest for $E_{G(1/4)}$. Considering that there is essentially no additional effort added for measuring E_G as compared to E_K and E_T, $E_{G(1/4)}$ is recommended.

B. Sound power measurement in a reverberation chamber

Sound power measurements based on the use of kinetic energy density or total energy density were also investigated by Nutter *et al.*[27] Their procedure is relatively simple and very similar to that based on the squared pressure method described in the ISO 3741 standard.[36] The spatially averaged sound level is the key parameter in the sound power estimation. In general, the more spatially uniform the sound field is, the fewer measurements are required to estimate the averaged sound level. The sound power measurement based on GED was investigated experimentally with the same equipment and in the same reverberation chamber described in the previous section. With the source being placed close to a corner in the reverberation chamber (the source was about 1.5 m away from the floor and walls), the GED field was sampled with the microphone gradient probe at six well separated locations (at least 1.5 m apart). The locations were randomly chosen with the constraint of being at least 1.5 m from the source and the walls. Figure 10(a) shows the averaged GED levels, which can be calculated as $L_G = 10\log(E_G/E_{G\mathrm{ref}})$, where $E_{G\mathrm{ref}} = (20\mu Pa)^2/(2\rho_0 c^2)$. The agreement among different α values is good below the 1 kHz one-third-octave band. Above that frequency, the estimations diverge due to the increased errors caused by the pressure gradient technique. The large difference at 100 Hz

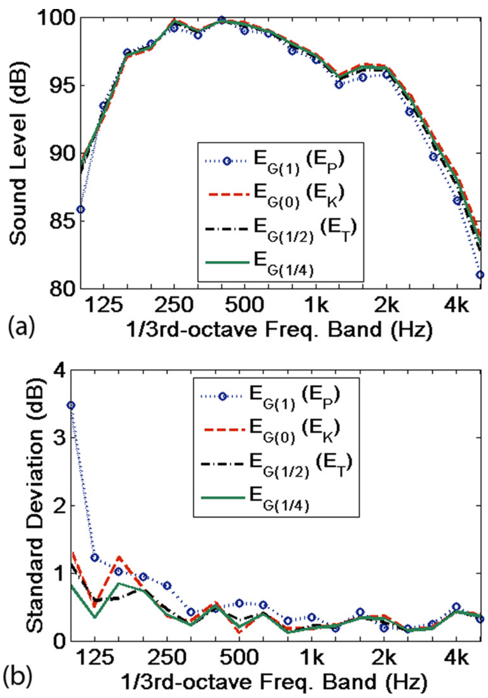

FIG. 10. (Color online) Sound level data for sound power measurements using GED. (a) Spatially averaged sound levels for different GED quantities in a reverberation chamber where the source under test is placed in a corner and 1.5 m away from the floor and walls. (b) Standard deviation of sound levels for the different source-receiver locations.

is caused by the large variance for the sound level of E_P. This can be seen in Fig. 10(b), which shows the standard deviation of the sound level for different measurement locations and different GED α values. Again, less variance for GED with $\alpha < 1$ can be observed, especially in the low-frequency range. In general, the sound level of $E_{G(1/4)}$ has the smallest standard deviation, but the improvement is not too dramatic when compared to E_K and E_T. However $E_{G(1/4)}$ is again recommended due to its improved uniformity with a measurement effort similar to those of E_T and E_K.

For the results presented here, the focus is on comparing results obtained using GED with various values of α. It should be noted that earlier work[27] in the same reverberation chamber provided an extensive comparison of results obtained using pressure measurements and total acoustic energy density measurements. That work indicated that for applications where spatial uniformity is desirable, energy density-based measurements are generally preferable to pressure measurements. The results presented here provide guidance as to what value of α can be expected to yield the best results for GED-based measurements.

C. Global active noise cancellation (ANC) in the low-frequency range of an enclosure

In a lightly damped enclosure, the total acoustic potential energy can be reduced at resonance frequencies below the Schroeder frequency by actively minimizing the squared acoustic pressure at error sensor locations using one or more secondary sources.[37–39] However, for given primary and secondary source locations, the global attenuation may vary over a large range for different error sensor placements. At off resonance frequencies, negative attenuation can often be observed. There is an upper-bound limit for the attenuation that can be achieved by minimizing the global acoustic potential energy. However, in principle, this requires an infinite number of error sensors placed in the enclosure. If, instead of squared pressure, the total acoustic energy density is minimized at discrete locations, the undesirable effects of the error sensor positions can be reduced.[19,26] With the same number of error sensors, the global attenuation of the total-energy-density-based ANC is closer to the upper bound limit than the squared-pressure-based ANC.

TABLE II. Room modes of a lightly damped enclosure (dimensions: 2.7 m × 3 m × 3.1 m).

Mode	(0,0,1)	(1,2,0)	(0,0,2)	(2,0,1)	(1,2,1)	(1,1,2)
Modal frequency (Hz)	54.59	126.10	126.18	126.70	138.45	138.53

In this section, the active noise cancellation based on GED in a lightly damped enclosure is simulated numerically. The dimensions of the enclosure are 2.7 m × 3.0 m × 3.1 m and a few of the normal modes are listed in Table II. One of the corners of the enclosure sits at the origin with the three adjoining edges lying along the positive directions of the x, y, and z axes. One primary source is located close to a corner at $(0.27\ \text{m}, 0.3\ \text{m}, 0.31\ \text{m})$, and one secondary source is located at $(2.2\ \text{m}, 2.0\ \text{m}, 0.94\ \text{m})$. One error sensor is randomly placed in the enclosure with the only constraint being that it is at least one wavelength away from both sources. One

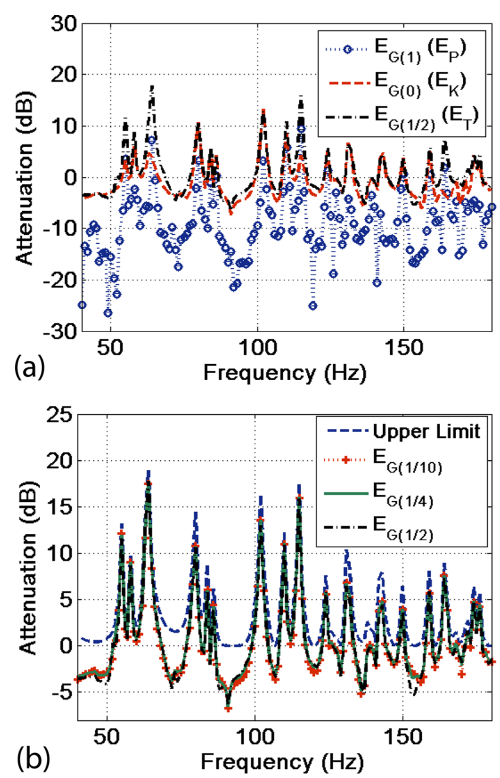

FIG. 11. (Color online) Average global attenuation using GED-based active noise cancellation in an enclosure with random error sensor locations. (a) Average attenuation based on $E_{G(1)}$ (E_P), $E_{G(0)}$ (E_K) and $E_{G(1/2)}$ (E_T). (b) Average attenuation based on $E_{G(1/2)}$, $E_{G(1/4)}$, $E_{G(1/10)}$ and the total potential energy upper-bound limit. The attenuation based on total potential energy is considered optimal (Ref. 37).

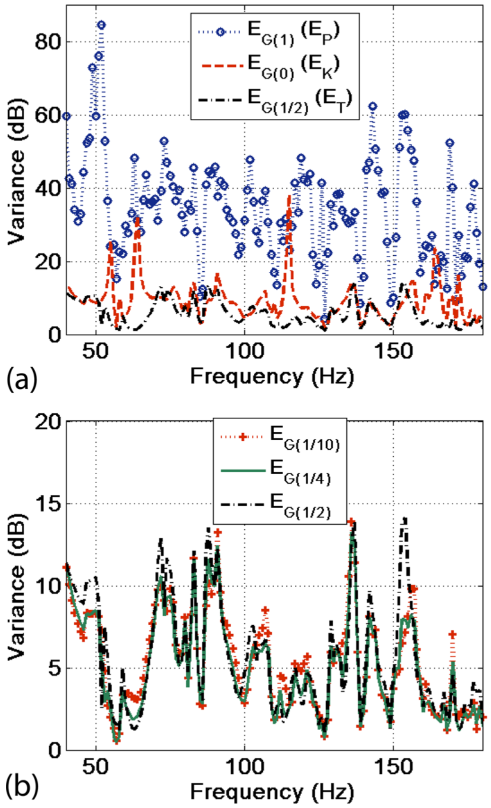

FIG. 12. (Color online) Variance of the attenuation. (a) Variance of the attenuation for $E_{G(1)}$ (E_P), $E_{G(0)}$ (E_K), and $E_{G(1/2)}$ (E_T). (b) Variance of the attenuation for $E_{G(1/2)}$, $E_{G(1/4)}$, and $E_{G(1/10)}$.

hundred tests were performed, with the secondary source strength being adjusted each time to minimize GED at the randomly chosen error sensor location. The bandwidth of 40 to 180 Hz was studied, with 1 Hz increments. The average attenuation over the tests of the total potential acoustic energy in the enclosure was compared for the various control schemes. As shown in Fig. 11(a), the E_T-based ANC is notably better than the E_P-based ANC and slightly better than the E_K based ANC. The E_P (or squared pressure) based ANC can result in large boosts (negative attenuation) for off resonance frequencies, while the E_K and E_T-based ANC result in much smaller boosts. Figure 11(b) compares GED-based ANC for the α values of $1/10$, $1/4$, and $1/2(E_T)$, along with the upper bound limit. These three ANC results are very similar. The $E_{G(1/4)}$-based ANC tends to achieve a slightly better attenuation than the other two. The difference, however, is small except for the frequencies around 154 Hz. It can also be observed that the $E_{G(1/4)}$-based ANC generally has less attenuation variance than the other schemes (Fig. 12).

VIII. CONCLUSIONS

Generalized acoustic energy density (GED) has been introduced in this paper. When averaged over the volume of an enclosure, it has the same mean value as the acoustic total energy density. It can revert to the traditional energy density quantities, such as acoustic potential energy density, acoustic kinetic energy density, and acoustic total energy density. By varying its weighting factors for the combination of acoustic potential energy density and acoustic kinetic energy density, an additional degree of freedom is added to the summed energy density quantity so that it can be optimized for different applications. Properties of GED with different values of α have been studied for individual room modes, diffuse sound fields, and sound fields below the Schroeder frequency.

The uniformity of a measured sound field often plays an important role in many applications. This work has shown that optimal weighting factors based on a single parameter α can minimize the spatial variance of the GED. For a single room mode, the optimal value of α may vary from $1/10$ to $1/2$, depending on the specific mode shape. For a diffuse field, the optimal value is $1/4$ for both single frequency and narrow-band frequency excitations, even for the region close to a rigid reflecting surface. For a diffuse field excited by a single tone source, $E_{G(1/4)}$ follows the distribution of $\Gamma(4, \mu_G/4)$ and has a relative spatial variance of $1/4$, compared to $1/3$ for E_K and E_T. Below the Schroeder frequency of a room, a smaller ensemble variance can also be reached when $\alpha = 1/4$.

Benefits of total-energy-density-based techniques have been shown in the past. Experimental studies of GED-based reverberation time and sound power measurements in a reverberation chamber confirm the improved uniformity of $E_{G(1/4)}$, especially in the low-frequency region. They indicate that more reliable results may be obtained using $E_{G(1/4)}$ for those measurements. Global active noise control in a lightly damped enclosure has also been studied through computer simulation. The results demonstrated that when $\alpha \le 1/2$, the average global attenuation is not particularly sensitive to the specific value of α, but $E_{G(1/4)}$ introduces less variance for the attenuation than other quantities.

In general, $E_{G(1/4)}$ based techniques do result in improvements compared to E_T and E_P based techniques. The degree of the improvements were not large compared to the E_T-based techniques. However, since $E_{G(1/4)}$ requires no additional effort to implement in most applications, and since it is very simple to modify existing E_T-based techniques, the $E_{G(1/4)}$-based techniques may be considered to be superior.

[1] W. C. Sabine, *Collected Papers on Acoustics* (Dover Publications, New York, 1964), p. 279.

[2] I. Wolff and F. Massa, "Direct meaurement of sound energy density and sound energy flux in a complex sound field," J. Acoust. Soc. Am. **3**, 317–318 (1932).

[3] I. Wolff and F. Massa, "Use of pressure gradient microphones for acoustical measurements," J. Acoust. Soc. Am. **4**, 217–234 (1933).

[4] L. W. Sepmeyer and B. E. Walker, "Progress report on measurement of acoustic energy density in enclosed spaces," J. Acoust. Soc. Am. **55**, S12 (1974).

[5] R. V. Waterhouse, "Statistical properties of reverberant sound fields," J. Acoust. Soc. Am. **43**, 1436–1444 (1968).

[6] R. H. Lyon, "Statistical analysis of power injection and response in structures and rooms," J. Acoust. Soc. Am. **45**, 545–565 (1969).

[7] R. K. Cook and P. A. Schade, "New method for measurement of the total energy density of sound waves," *Proc. Inter-Noise* 74, Washington, DC, 1974, pp. 101–106.

[8] R. V. Waterhouse and R. K. Cook, "Diffuse sound fields: Eigenmode and free-wave models," J. Acoust. Soc. Am. **59**, 576–581 (1976).

[9] R. V. Waterhouse and D. W. v. W. Palthe, "Space variance for rectangular modes," J. Acoust. Soc. Am. **62**, 211–213 (1977).

[10] F. Jacobsen, "The diffuse sound field: statistical considerations concerning the reverberant field in the steady state," Technical Report, Technical University of Denmark, 1979.

[11]J. A. Moryl and E. L. Hixson, "A total acoustic energy density sensor with applications to energy density measurement in a reverberation room," *Proc. Inter-Noise* 87, Beijing, China, Vol. II, pp. 1195–1198.
[12]J. A. Moryl, "A study of acoustic energy density in a reverberation room," Ph.D. thesis, The University of Texas at Austin (1987).
[13]R. L. Weaver and J. Burkhardt, "Weak Anderson localization and enhanced backscatter in reverberation rooms and quantum dots," J. Acoust. Soc. Am. **96**, 3186–3190 (1994).
[14]F. Jacobsen and A. R. Molares, "Sound power emitted by a pure-tone source in a reverberation room," J. Acoust. Soc. Am. **126**, 676–684 (2009).
[15]F. Jacobsen and A. R. Molares, "The ensemble variance of pure-tone measurements in reverberation rooms," J. Acoust. Soc. Am. **127**, 233–237 (2010).
[16]J. L. Davy, "The relative variance of the transmission function of a reverberation room," J. Sound Vib. **77**, 455–479 (1981).
[17]R. L. Weaver, "On the ensemble variance of reverberation room transmission functions, the effect of spectral rigidity," J. Sound Vib. **130**, 487–491 (1989).
[18]F. Jacobsen and A. R. Molares, "Statistical properties of kinetic and total energy densities in reverberant spaces," J. Acoust. Soc. Am. **127**, 2332–2337 (2010).
[19]J. W. Parkins, S. D. Sommerfeldt, and J. Tichy, "Error analysis of a practical energy density sensor," J. Acoust. Soc. Am. **108**, 211–222 (2000).
[20]B. S. Cazzolato and C. H. Hansen, "Errors arising from three-dimensional energy density sensing in one-dimensional sound fields," J. Sound Vib. **236**, 375–400 (2000).
[21]J. Ghan, B. Cazzolato, and S. Snyder, "Statistical errors in the estimation of time-averaged acoustic energy density using the two-microphone method," J. Acoust. Soc. Am. **115**, 1179–1184 (2004).
[22]J.-C. Pascal and J.-F. Li, "A systematic method to obtain 3d finite-difference formulations for acoustic intensity and other energy quantities," J. Sound Vib. **310**, 1093–1111 (2008).
[23]H.-E. de Bree, P. Leussink, T. Korthorst, H. Jansen, T. S. J. Lammerink, and M. Elwenspoek, "The u-flown: A novel device for measuring acoustic flows," Sens. Actuators A, **54**, 552–557 (1996).
[24]T. G. H. Basten and H.-E. de Bree, "Full bandwidth calibration procedure for acoustic probes containing a pressure and particle velocity sensor," J. Acoust. Soc. Am. **127**, 264–270 (2010).
[25]J. W. Parkins, "Active minimization of energy density in a three-dimensional enclosure," Ph.D. thesis, The Pennsylvania State University (1998).
[26]J. W. Parkins, S. D. Sommerfeldt, and J. Tichy, "Narrowband and broadband active control in an enclosure using the acoustic energy density," J. Acoust. Soc. Am. **108**, 192–203 (2000).
[27]D. B. Nutter, T. W. Leishman, S. D. Sommerfeldt, and J. D. Blotter, "Measurement of sound power and absorption in reverberation chambers using energy density," J. Acoust. Soc. Am. **121**, 2700–2710 (2007).
[28]P. M. Morse and R. H. Bolt, "Sound waves in rooms," Rev. Mod. Phys. **16**, 69–150 (1944).
[29]D. Lubman, "Fluctuations of sound with position in a reverberant room," J. Acoust. Soc. Am. **44**, 1491–1502 (1968).
[30]R. K. Cook, R. V. Waterhouse, R. D. Berendt, S. Edelman, and J. M. C. Thompson, "Measurement of correlation coefficients in reverberant sound fields," J. Acoust. Soc. Am. **27**, 1072–1077 (1955).
[31]D. Lubman, "Spatial averaging in a diffuse sound field," J. Acoust. Soc. Am. **46**, 532–534 (1969).
[32]S. J. Elliott, P. Joseph, A. J. Bullmore, and P. A. Nelson, "Active cancellation at a point in a pure tone diffuse sound field," J. Sound Vib. **120**, 183–189 (1988).
[33]R. V. Waterhouse, "Interference patterns in reverberant sound fields," J. Acoust. Soc. Am. **27**, 247–258 (1955).
[34]B. Xu and S. D. Sommerfeldt, "A hybrid modal analysis for enclosed sound fields," J. Acoust. Soc. Am. **128**, 2857–2867 (2010).
[35]M. R. Schroeder, "New method of measuring reverberation time," J. Acoust. Soc. Am. **37**, 409–412 (1965).
[36]ISO 3741:1999(E), "Acoustics—Determination of sound power levels of noise sources using sound pressure—Precision methods for reverberation rooms" (International Organization for Standardization, Geneva, 1999).
[37]P. A. Nelson, A. R. D. Curtis, S. J. Elliott, and A. J. Bullmore, "The active minimization of harmonic enclosed sound fields, part I: Theory," J. Sound Vibr. **117**, 1–13 (1987).
[38]A. J. Bullmore, P. A. Nelson, A. R. D. Curtis, and S. J. Elliott, "The active minimization of harmonic enclosed sound fields, part II: A computer simulation," J. Sound Vibr. **117**, 15–33 (1987).
[39]S. J. Elliott, A. R. D. Curtis, A. J. Bullmore, and P. A. Nelson, "Active minimization of harmonic enclosed sound fields, part III: Experimental verification," J. Sound Vibr. **117**, 35–58 (1987).